Advances in Science and Technology Research Journal

Advances in Science and Technology Research Journal, 2025, 19(1), 381–389
https://doi.org/10.12913/22998624/195755
ISSN 2299-8624, License CC-BY 4.0

Received: 2024.08.12
Accepted: 2024.11.15
Published: 2024.12.01

The effects of atmospheric plasma spray parameters on structure and mechanical properties of titanium dioxide coatings

Karolina Płatek[1*], Leszek Łatka[1], Paweł Sokołowski[1], Tomasz Kiełczawa[1], Adam Sajbura[1]

[1] Department of Metal Forming, Welding and Metrology, Faculty of Mechanical Engineering, Wroclaw University of Science and Technology, Wroclaw, Poland
* Corresponding author's e-mail: karolina.platek@pwr.edu.pl

ABSTRACT

Titanium dioxide (TiO_2) coatings, renowned for their photocatalytic properties, are of significant interest for environmental and industrial applications. This study investigates the deposition of black titanium oxide (BTO)-containing coatings using the atmospheric plasma spraying (APS) process, employing an argon-hydrogen plasma mixture. The influence of hydrogen flow rate, spray distance, and powder feed rate on the structure and mechanical properties of the resulting coatings was examined. Deposited coatings were examined in terms of their structure, thickness porosity and specific surface area. Examination of the mechanical properties included hardness test and Young's modulus measurement. Presence of partially sintered fine droplets was revealed by SEM observations and mechanism of their formation was discussed. The examination of mechanical properties showed that within the examined parameters, spray distance has the greatest impact on Young's modulus, hardness and porosity of the coatings, while the powder feed rate affects coatings thickness.

Keywords: thermal spraying, hydrogenated TiO_2, BTO, photocatalytic coating, mechanical properties.

INTRODUCTION

Among various metal oxides, TiO_2 draws a special attention from both scientific and manufacturing industries due to its high chemical and physical stability, non-toxicity and photocatalytic properties [1, 2]. However, the bandgap value of TiO_2, which is 3.2 eV for anatase and 3.0 eV for rutile, is too large to enable photocatalysis under visible (VIS) light irradiation [3]. In 2011, Chen et al. demonstrated that hydrogenated TiO_2 exhibits enhanced photocatalytic activity compared to non-treated material [4]. Hydrogenated TiO_2, often referred to as black titanium oxide (BTO) due to the color of reduced titanium oxide, has immediately gained an attention from the scientific community. The investigations focus also on its manufacturing methods. Methods such as hydrogen thermal treatment [5], chemical or electrochemical reduction [6], and anodization-annealing [7] have been tested and proven effective. However, most of these methods are time-consuming and not cost-effective, hindering their implementation in the manufacturing industry.

As an alternative, thermal spraying methods are currently being researched with highly promising results [8, 9]. In this process, the feedstock material is introduced into the plasma stream. If the feedstock is in powder form, the process is called atmospheric plasma spraying (APS). Particles properly introduced into the plasma stream undergo partial or full melting due to the high temperatures of plasma gases, which can reach up to 20,000 K. Highly plasticized particles, accelerated by gases, reach the substrate and deform upon impact, forming a lamella structure called a "splat." A mixture of argon with an addition of nitrogen or helium is usually used as plasma gases.

However, nitrogen can be replaced by hydrogen with minor impacts on process characteristics [10]. Due to the high dissociation and ionization peaks of H_2, adding hydrogen significantly increases the thermal conductivity of the mixture [11]. Consequently, the feedstock is heated extensively, which, along with the hydrogen-rich atmosphere, induces chemical reduction of the TiO_2 powder, forming oxygen vacancies and Ti^{3+} species. As a result, a coating with a high content of BTO is deposited in a relatively simple, one-step process [12].

However, the use of thermal spray methods for BTO deposition are still undeveloped. To fully use the potential of plasma spraying for BTO deposition, it is needed to examine the impact of process parameters on both structural and mechanical properties of the coatings, as they are crucial for its functionality [13]. Since photocatalytic reaction occur on the materials surface, specific surface area (SSA) of the coating has a significant influence on its efficiency [14]. Thus, it is important to determine the impact of process parameters on this property. Input power, plasma gas flow rate, and spray distance are often defined as the most crucial process parameters [15, 16]. Both input power and gas flow rate influence the temperature of the plasma stream. Increasing plasma temperature leads to increased coating density and better cohesion, which often translates to improved anti-wear characteristics [16]. On the other hand, spray distance affects the time particles spend in the plasma stream, impacting their temperature [17]. Additionally, the feedstock feeding rate is crucial for process efficiency [18]. Understanding the relationship between process parameters and the structure of BTO coating is essential for effective deposition of the coatings.

In the presented research, the impact of hydrogen flow rate, spray distance, and feedstock feeding rate on the structure and mechanical properties of BTO coatings was examined. Commercially available TiO_2 powder was used as the feedstock. The deposited coatings were analyzed in terms of their structure, thickness, porosity, and specific surface area. Mechanical properties were evaluated through hardness tests and Young's modulus measurements.

MATERIALS AND METHODS

The samples were prepared from Metco 102 powder (Oerlikon, Metco) using one-cathode – one anode SG-100 plasma torch (Praxair, Indianapolis, In, USA), attached to a 6-axis Fanuc 2000 IA robot. An Ar/H_2 gas mixture with various ratios was used for plasma generation. The hydrogen flow varied from 2.5 to 5.0 slpm, while the Ar flow was kept constant at 50.0 slpm. In addition to hydrogen content, powder feeding rate and spraying distance were also varied. All variable spraying parameters and their corresponding sample codes are listed in Table 1. The voltage was set on 50 V. The choice of process parameters was based on preliminary studies as well as previous works with similar materials [19, 20].

The coatings were deposited on 1.4301 austenitic stainless-steel discs with a diameter of 25 mm and a thickness of 2 mm. Prior to spraying, the discs were sandblasted with F40 corundum grit (according to FEPA standards) and cleaned using an ultrasonically assisted ethanol bath. After sandblasting, the surface roughness (Ra) was approximately 5 μm. During deposition, the plasma torch was mounted on a 6-axis Fanuc 2000 IA

Table 1. Variable parameters and corresponding sample codes

Sample code	Variable parameters		
	Hydrogen flow, slpm	Powder feed rate, g/min	Spray distance, mm
TA1	2.5	10	90
TA2	2.5	10	110
TA3	2.5	20	90
TA4	2.5	20	110
TA5	5.0	10	90
TA6	5.0	10	110
TA7	5.0	20	90
TA8	5.0	20	110
TA9	3.75	15	100

robot, and the substrates were positioned on a rotating carousel, as shown in Figure 1.

The feedstock material was examined for size and morphology using a PSA 1190 particle size analyser (Anton Paar, Graz, Austria) and SEM (Tescan Vega 3 (Tescan, Brno, Czech Republic). After deposition, the structure and morphology of the coatings were observed using digital microscope Keyence VHX 6000 (Keyence, Mechelen, Belgium) and SEM. The Keyence software was used for the measurement pecific surface area (SSA) of the coatings based on the free surface characteristicts. Observations performed on coatings cross-sections were further used for thickness and porosity measurements. Porosity was assessed from SEM BSE images using an automated analysis algorithm (ASTM E2109-01, method B) [22]. For each sample, 25 images were taken and the average porosity was calulated based on binarized pictures.

The mechanical properties of the deposited coatings were assessed by Vickers hardness measurement and indentation tests. The Vickers hardness measurement was carried out in accordance with the EN ISO 4516 standard using a Sinowon HV-1000 apparatus (Sinowon Innovation Metrology, China) [23]. For each sample, 12 imprints were made under a load of 1.96 N (HV0.2). The indentation tests were performed using an NHT^3 nanoindenter (Anton Paar, Graz, Austria) equipped with a Berkovich indenter. To determine the Young's modulus of the coatings, a series of measurements under various loads was made following the ASTM E2546 standard [24].

RESULTS AND DISCUSSION

The particle size distribution is presented in Figure 2a. The particle sizes correspond with the

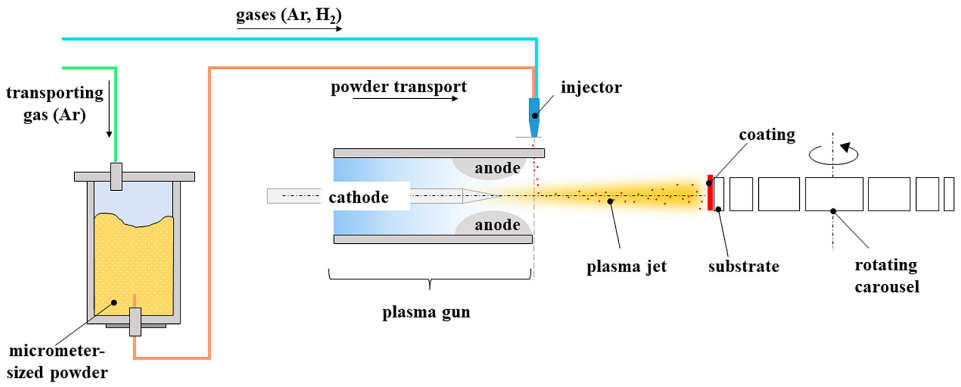

Figure 1. Configuration of deposition system based on [21]

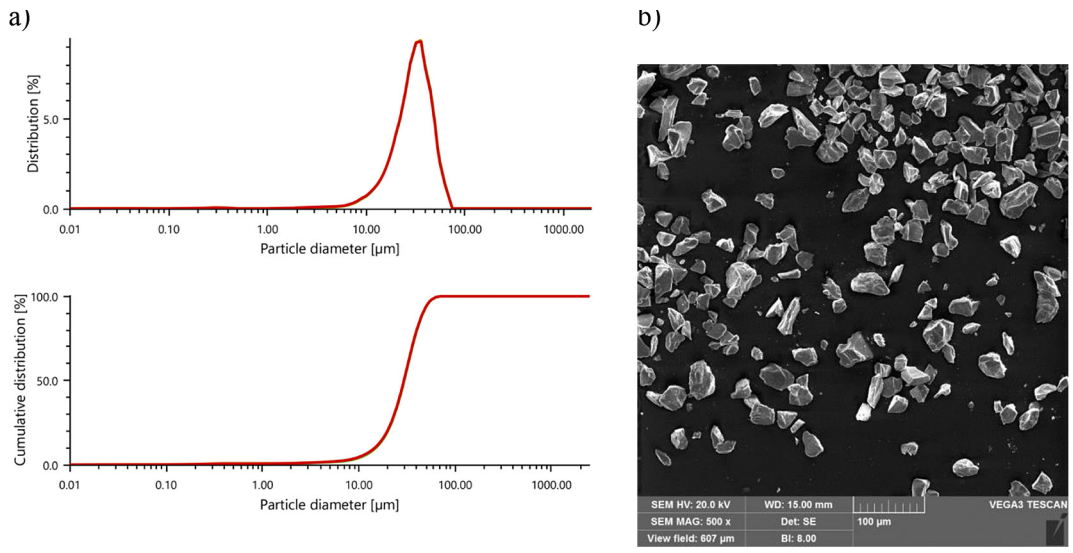

Figure 2. Result of feedstock analysis: a) distribution and cumulative distribution of particle size, b) SEM observation of powders morphology

manufacturer's specifications, with a d_{50} = 29.5 ± 0.1 µm and a mean size of 31.6 ± 0.2 µm. SEM observation of feedstock powder (Figure 2b) revealed that the powder has an irregular geometry, typical for its manufacturing methods (fused and crushed). In the SEM images, a fraction of small-sized particles is visible, but their presence is not represented in the results particle size analysis due to their minimal quantity.

Observations using a digital microscope revealed delamination of the TA2 coating from the substrate (Figure 3a). Delamination occurs when the adhesion between the coating and the substrate is insufficient. This may be due to low surface roughness relative to the size of the feedstock particles or high stresses during the deposition process. Since the preparation procedure and feedstock material were consistent across all samples, the delamination is most likely related to the spray parameters. It is suspected that low heat input, connected to the H_2 content, combined with spray distance of 110 mm led to in-flight particle solidification. Consequently, particles of low plasticity and kinetic energy were unable to attach themselves firmly to the substrate, what was exposed during the preparation procedure. No other imperfections were observed in any of the deposited coatings.

The thickness of the coatings, measured using a digital microscope (Figure 3b), ranged from 100 ± 7 µm for sample TA6 to 139 ± 9 µm for sample TA9. The results are shown in Figure 4a. The powder feed rate had a clear impact on coating thickness. The average thickness of coatings deposited with a powder feed rate of 10 g/min was 104.8 ± 4.6 µm, while a feed rate of 20 g/min resulted in average thicknesses of 128.8 ± 4.4. However, the thickest coating was TA9, which was deposited with a feed rate of 15 g/min. Although the difference in thickness between sample TA9 and sample TA8 is only 3 µm, what falls within the range of standard deviation.

According to the porosity measurements (Figure 4b), the porosity of the deposited coatings ranges from 2.13% to 3.89%. According to the literature [25], this level of porosity is typical or even low for this manufacturing technique. A slight correlation between coating porosity and spraying distance was observed, with greater spray distances resulting in higher porosity levels. However, this correlation does not apply to sample TA3, which exhibits the highest porosity level among all samples. The porosity of sample TA3 was 3.89%, followed by sample TA6 with a porosity of 3.72%. The high porosity level of sample TA3 is likely due to insufficient heating of the particles, caused by a low hydrogen level and a high spray distance, which allowed for particle resolidification. However, due to the high standard deviation, this conclusion cannot be definitive.

The SSA of the coatings ranged from 0.79 to 1.44 m^2/g (Figure 5). The highest SSA was measured for the sample TA6, which was sprayed using 5 slpm of H_2 from the distance of 60 mm with the 10 g/min powder feed. It can be also seen that the opposite process parameters (lower H_2 content, lower spray distance and higher powder feed rate) resulted in the lowest SSA. Among tested ranges, the spray distance has the highest influence on SSA value. Decreasing of the SD usually leads to formation of denser coatings, what explains its relationship with SSA, as in most of the cases, the SSA value is correlated with the porosity. The exemption is TA3 sample, which high

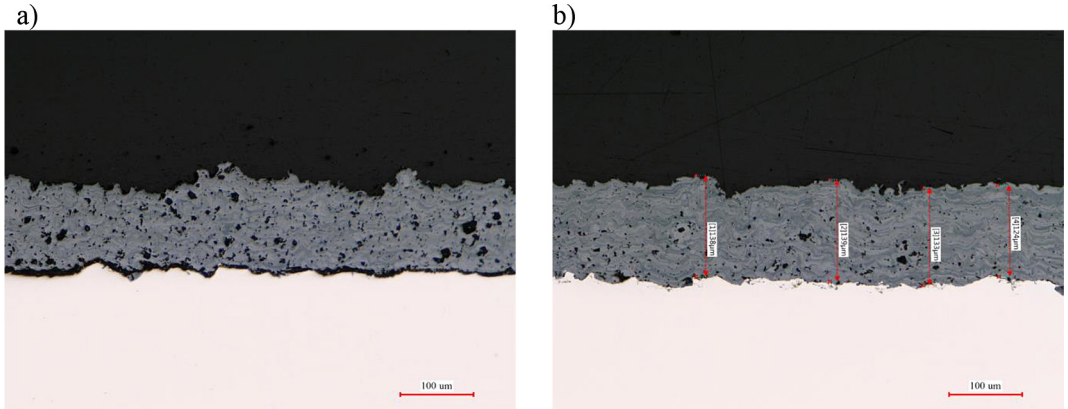

Figure 3. Coatings cross-section observed using digital microscope: a) delamination of TA2 coating; b) thickness measurement of TA8 sample

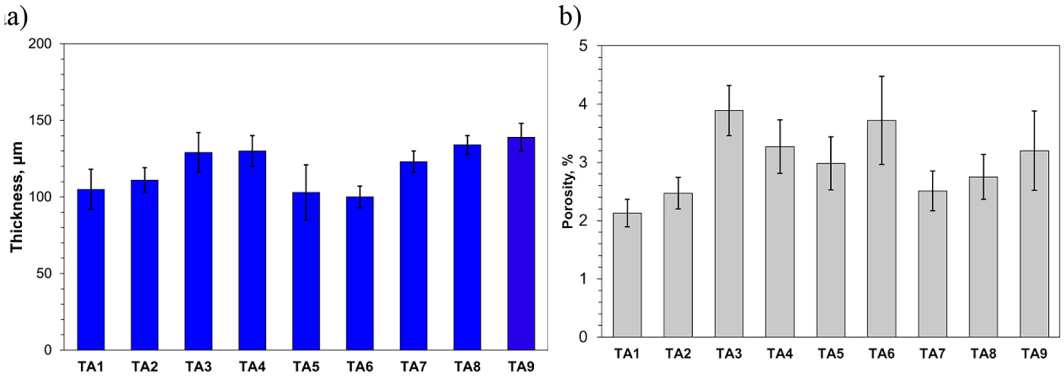

Figure 4. a) Thickness and b) porosity of the coatings

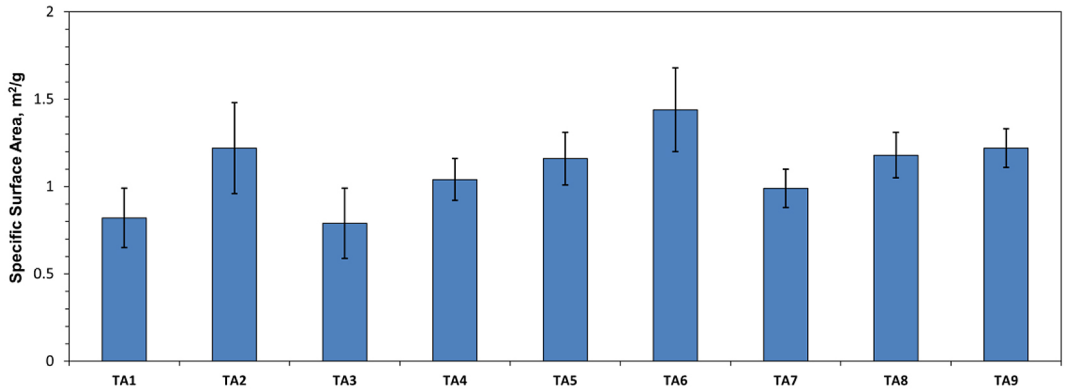

Figure 5. The SSA of the coatings

porosity did not contribute to high SSA, since the largest pores were located near the substrate.

The surface structure of the deposits, as observed using SEM, displays several characteristic features typical of Atmospheric Plasma Spraying (APS) coatings, including various types of splats, cracks, and pores. Most of the splats were identified as flower-like, with a minor presence of disc-like splats. The formation of these splat types is strongly influenced by process conditions, particularly substrate temperature, which significantly affects coating properties. Wan et al. [26] stated that low substrate temperatures lead to rapid and uneven cooling, beginning at the edges of the splats. If the central zone of the splat remains molten, the force of the liquid can cause it to jet over the solidified perimeter, resulting in a distorted structure with numerous small droplets and occasional voids in the center. This phenomenon, known as freezing-induced break-up, is described in detail in [27–29]. With the increase in substrate temperature the shape of the splat's changes from an irregular to a disc-like. The temperature, at which it takes place, is called transition temperature (T_t). According to Mutter et al. [30], disc-like splats are preferable because flower-like splats can reduce coating cohesion. In the examined case, despite application of the preheating, most of the splats undergo fragmentation, indicating that the substrate temperature was below the transition temperature.

Apart from freezing-induced break-up, the presence of small particles may result from in-flight particle break up. When introduced into the plasma stream, the particles are exposed to high temperatures and velocities, which can sometimes cause them to break up into smaller droplets. This phenomenon is particularly likely when the initial powder particles have an irregular shape, as is common with powders produced by fusing and crushing [31]. When the spray distance is large enough, particles can resolidify, with smaller particles being especially prone to this due to their high surface-to-volume ratio. Consequently, a large number of small, resolidified particles reach the substrate and attach to its surface as small spheres, as can be seen in Figure 3a. This phenomenon was observed in all deposited coatings. However, in the case of coatings sprayed from a distance of 90 mm, the particles are much more deformed (Figure 3b),

suggesting that solidification was not complete when they reached the surface.

As can be seen in Figure 6, larger splats are marked with cracks across their surface. Cracking in thermally sprayed coatings is usually associated with high intrinsic stresses resulting from rapid cooling [32]. The number of cracks observed on the coating surface is noticeably higher in samples sprayed from 90 mm compared to those deposited with a spray distance of 110 mm. Moreover, in the former case, the cracks appear much darker, indicating greater depth.

What is more, SEM observations revealed the presence of splats formed from partially melted agglomerates of nano-sized particles. Agglomerated splats were found in all our coatings, indicating no correlation with the spraying parameters within the examined ranges. We assume that these splats form as a result of in-flight particle break-up, followed by in-flight agglomeration and partial sintering of nano-sized particles. Heat transfer in sintered particles is lower than in bulk particles, causing the interior region to remain solid during impact, while the peripheral area melts, allowing the splat to form. Additionally, the degree of sintering of these agglomerated splats varies between samples, as well as within individual coatings. Examples of agglomerated splats at different sintering stages and schematic representation of this process are shown in Figure 7a-c. The proposed model of observed phenomenon is presented in Figure 7d. The model was developed based on our observations, as well as the literature reports on similar phenomena [33]. Similar structures were observed by Sathish et al. in [34], although the authors attributed their formation to the form of the initial powder, which was agglomerated and sintered. Since there were no agglomerated particles in our initial feedstock powder, we assume that the agglomeration process occurred spontaneously during spraying. This phenomenon is common in plasma spraying with nano-sized particles and has been extensively described by Pawlowski [35].

The hardness of the samples ranged from 730 ± 102 to 868 ± 91 HV0.2. Although a slight correlation between spray distance and hardness can be observed (with an increase in spray distance generally leading to an increase in hardness), this trend is not particularly strong. The Young's modulus values showed small deviations among the samples, ranging from 206 to 216 GPa. Similar to thickness, porosity, and hardness, spray distance appears to have the strongest influence on this property among the parameters tested. For each pair of samples that differed only by spray distance, a shorter spray distance resulted in a higher Young's modulus. The variations in elastic modulus are likely connected to differences in phase composition, as TiO_2 undergoes an irreversible transition from the metastable anatase phase to the stable rutile phase under the influence of heat. The exact values of these characteristics are listed in Table 2.

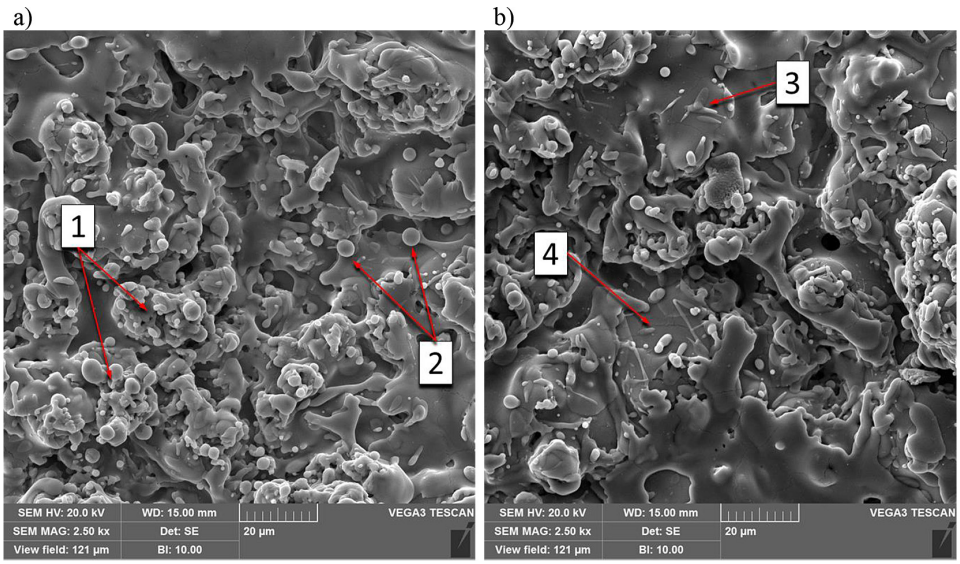

Figure 6. Surface of the coatings observed using SEM microscope: a) sample TA2 and characteristic structures: 1 – agglomerates of small particles, 2 – small, resolidified particles; b) sample TA7: 3 – small, deformed particles being a result of incomplete in-flight solidification and 4 – cracks on the splats surface

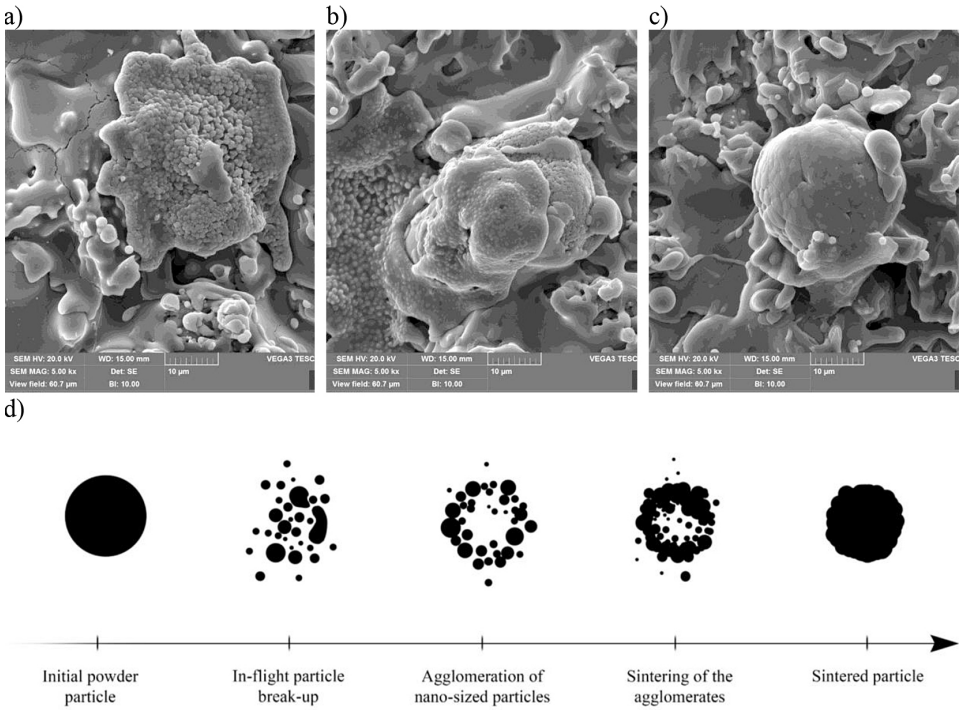

Figure 7. Agglomerated splats at different stages of sintering: a) partially sintered splats with visible difference in sintering stage between splats interior and peripheries; b) agglomeration of sintered splats; c) spheroidal particle formed from sintered droplets; d) proposed model of the phenomenon.

Table 2. Hardness and Young's modulus of the coatings

Sample	Mechanical properties	
	Hardness, HV0.2	Young's modulus, GPa
TA1	760 ± 107	212 ± 6
TA2	789 ± 70	208 ± 6
TA3	826 ± 97	210 ± 8
TA4	818 ± 67	206 ± 8
TA5	756 ± 95	216 ± 7
TA6	831 ± 75	209 ± 8
TA7	730 ± 102	215 ± 6
TA8	868 ± 91	207 ± 7
TA9	830 ± 99	211 ± 7

CONCLUSIONS

Titania-based coatings are the focus of intensive research due to their exceptional photocatalytic properties. This study explored the deposition of black titanium oxide (BTO)-containing coatings using the APS process with an argon-hydrogen plasma mixture. The coatings were deposited from commercially available Metco 102 powder, and the effects of various spraying parameters on the structure and mechanical properties of the coatings were investigated. Out of all deposited samples, only the TA2 sample exhibited visible delamination. This delamination was attributed to insufficient heating of the powder particles. The remaining samples did not show major imperfections, indicating effective adhesion.

The correlation between powder feed rate and coatings thickness is visible, although nonlinear. Even though the thickness of samples deposited with the feed rate of 20 g/min higher comparing to feed rate of 10 g/min, the highest thickness (139 µm) was obtained by sample deposited with the middle value of 15 g/min.

The porosity of the coatings increased with longer spray distances, although this trend was not uniform. Notably, the coating with the highest porosity level (TA3 at 3.89%) was deposited at a spray distance of 90 mm, which deviated from the general trend. On the other hand, spray distance had a significant impact on the specific surface area. The increase in spray distance, along with decrease of powder feed rate and increase in H_2 content led to deposition of coatings with SSA of 1.44 m^2/g.

SEM observations revealed the presence of particles with diameters significantly smaller than the initial powder. This was attributed to in-flight particle break-up and droplets resolidification and freezing-induced break-up. Longer spray distances resulted in droplets undergoing partial or full resolidification, leading to the formation of deformed or spheroidal particles on the coating surface. On the other hand, in contact with cold surface, splats tend to splash intensively forming an irregular structure surrounded with small droplets. Additionally, splats consisting of nano-sized in-flight sintered droplets were noticed.

Among tested variables, spray distance tends to have the greatest impact on hardness and Young's modulus. In most cases increase in spray distance results in increase in hardness and decrease in the value of Young's modulus. This effect is linked to the heat distribution and temperature variations of both the powder and substrate, which influence the phase transition of TiO_2.

Almost all deposited coatings fulfil requirements set for them in term of structure and mechanical properties. In further research, the influence of hydrogen flow rate on phase composition and photocatalytic activity of plasma sprayed coatings will be examined.

Acknowledgements

This work was supported by National Science Centre Poland, grant no. grant no. 2022/47/O/ST8/01066 Preludium BIS "Development of complex coatings with photocatalytic properties obtained by hybrid plasma spraying technologies".

REFERENCES

1. Isfa, B.; Jamarun, N.; Emriadi; Arief, S.; Ritonga, A.H.; Tanjung, D.A.; Sisca, V. Characterization and application of TiO_2/ZnO nanoparticles as pigments in matt-type water-based paint. International Journal of Technology 2023, 14, https://doi.org/10.14716/ijtech.v14i2.5501
2. Ghosh, S.; Das, A.P. Modified titanium oxide (TiO_2) nanocomposites and its array of applications: a review. Toxicol Environ Chem 2015, 97, https://doi.org/10.1080/02772248.2015.1052204
3. Kovačič, Ž.; Likozar, B.; Huš, M. Electronic properties of rutile and anatase TiO_2 and their effect on CO_2 adsorption: A comparison of first principle approaches. Fuel 2022, 328, 125322, https://doi.org/10.1016/J.FUEL.2022.125322
4. Chen, X.; Liu, L.; Yu, P.Y.; Mao, S.S. Increasing solar absorption for photocatalysis with black hydrogenated titanium dioxide nanocrystals. Science (1979) 2011, 331, 746–750, https://doi.org/10.1126/science.1200448
5. Wang, G.; Wang, H.; Ling, Y.; Tang, Y.; Yang, X.; Fitzmorris, R.C.; Wang, C.; Zhang, J.Z.; Li, Y. Hydrogen-treated TiO_2 nanowire arrays for photoelectrochemical water splitting. Nano Lett 2011, 11, 3026–3033, https://doi.org/10.1021/nl201766h
6. Xu, C.; Song, Y.; Lu, L.; Cheng, C.; Liu, D.; Fang, X.; Chen, X.; Zhu, X.; Li, D. Electrochemically hydrogenated TiO_2 nanotubes with improved photoelectrochemical water splitting performance. Nanoscale Res Lett 2013, 8, 391, https://doi.org/10.1186/1556-276X-8-391
7. Dong, J.; Han, J.; Liu, Y.; Nakajima, A.; Matsushita, S.; Wei, S.; Gao, W. Defective black TiO_2 synthesized via anodization for visible-light photocatalysis. ACS Appl Mater Interfaces 2014, 6, 1385–1388, https://doi.org/10.1021/am405549p
8. Ctibor, P.; Straka, L. Photoconductive TiO_2 dielectrics prepared by plasma spraying. Applied Sciences 2024, 14, https://doi.org/10.3390/app14051714
9. Wang, Q.; Tang, Z.; Herout, R.; Liu, C.; Yu, K.; Lange, D.; Godin, R.; Kizhakkedathu, J.N.; Troczynski, T.; Wang, R. Axial suspension plasma sprayed Ag-TiO_2 coating for enhanced photocatalytic and antimicrobial properties. Surfaces and Interfaces 2024, 45, 103856, https://doi.org/10.1016/j.surfin.2024.103856
10. Boulos, M.I.; Fauchais, P.L.; Heberlein, J.V.R. Thermal Spray Fundamentals: From Powder to Part, Second Edition; 2021.
11. Boulos, M.I.; Fauchais, P.L.; Pfender, E. Handbook of Thermal Plasmas; 2023.
12. Zhai, M.; Liu, Y.; Huang, J.; Wang, Y.; Chen, K.; Fu, Y.; Li, H. Efficient suspension plasma spray fabrication of black titanium dioxide coatings with visible light absorption performances. Ceram Int 2019, 45, 930–935, https://doi.org/10.1016/j.ceramint.2018.09.268
13. Maruszczyk, A.; Dudek, A.; Szala, M. Research into morphology and properties of TiO_2 – NiAl

Atmospheric plasma sprayed coating. Advances in Science and Technology Research Journal 2017, 11, 204–210, https://doi.org/10.12913/22998624/76450

14. Jung, S.C.; Kim, S.J.; Imaishi, N.; Cho, Y.I. Effect of TiO_2 thin film thickness and specific surface area by low-pressure metal–organic chemical vapor deposition on photocatalytic activities. Appl Catal B 2005, 55, 253–257, https://doi.org/10.1016/J.APCATB.2004.08.009
15. Aruna, S.T.; Balaji, N.; Shedthi, J.; Grips, V.K.W. Effect of critical plasma spray parameters on the microstructure, microhardness and wear and corrosion resistance of plasma sprayed alumina coatings. Surf Coat Technol 2012, 208, 92–100, https://doi.org/10.1016/J.SURFCOAT.2012.08.016
16. Song, E.P.; Ahn, J.; Lee, S.; Kim, N.J. Effects of critical plasma spray parameter and spray distance on wear resistance of Al_2O_3-8 Wt.%TiO_2 coatings plasma-sprayed with Nanopowders. Surf Coat Technol 2008, 202, https://doi.org/10.1016/j.surfcoat.2008.01.002
17. Tillmann, W.; Khalil, O.; Baumann, I. Influence of spray gun parameters on inflight particle's characteristics, the splat-type distribution, and microstructure of plasma-sprayed YSZ coatings. Surf Coat Technol 2021, 406, https://doi.org/10.1016/j.surfcoat.2020.126705
18. Gaur, A.; Pandel, U.; Sharma, S. A study of investigating the effects of variables and assessing the efficiency of air plasma spray as a coating technique. Mater Today Proc 2023, https://doi.org/10.1016/j.matpr.2023.11.096
19. Łatka, L.; Michalak, M.; Szala, M.; Walczak, M.; Sokołowski, P.; Ambroziak, A. Influence of 13 Wt% TiO_2 content in alumina-titania powders on microstructure, sliding wear and cavitation erosion resistance of APS sprayed coatings. Surf Coat Technol 2021, 410, 126979, https://doi.org/10.1016/J.SURFCOAT.2021.126979
20. Płatek, K.; Łatka, L.; Nowakowska, M. The influence of injection mode and spray distance on wear resistance of AlO+13 Wt.% TiO coatings. Advances in Materials Science 2024, 24, 5–17, https://doi.org/10.2478/adms-2024-0014
21. Michalak, M.; Łatka, L.; Sokołowski, P.; Niemiec, A.; Ambroziak, A. The microstructure and selected mechanical properties of Al_2O_3 + 13 Wt % TiO_2 plasma sprayed coatings. 2020, 10, 173, https://doi.org/10.3390/coatings10020173
22. ASTM International ASTM E2109-01: Standard Test Methods for Determining Area Percentage Porosity in Thermal Sprayed Coatings. Book of Standard 2021, https://doi.org/10.1520/E2109-01R21
23. EN ISO 4516: Metallic and Other Inorganic Coatings – Vickers and Knoop Microhardness Tests; Swiss Association for Standardization; Winterthur, Switzerland, 2004.
24. ASTM International ASTM E2546-15: Standard Practice for Instrumented Indentation Testing. Book of Standards 2023, 03.01.
25. Odhiambo, J.G.; Li, W.; Zhao, Y.; Li, C. Porosity and Its Significance in Plasma-Sprayed Coatings. Coatings 2019, 9, 460, https://doi.org/10.3390/coatings9070460
26. Wan, Y.P.; Zhang, H.; Jiang, X.Y.; Sampath, S.; Prasad, V. Role of solidification, substrate temperature and reynolds number on droplet spreading in thermal spray deposition: measurements and modeling. J Heat Transfer 2000, 123, 382–389, https://doi.org/10.1115/1.1351893
27. Dhiman, R.; McDonald, A.G.; Chandra, S. Predicting splat morphology in a thermal spray process. Surf Coat Technol 2007, 201, 7789–7801, https://doi.org/10.1016/j.surfcoat.2007.03.010
28. Sampath, S.; Jiang, X.Y.; Matejicek, J.; Leger, A.C.; Vardelle, A. Substrate temperature effects on splat formation, microstructure development and properties of plasma sprayed coatings part I: Case Study for Partially Stabilized Zirconia. Materials Science and Engineering: A 1999, 272, 181–188, https://doi.org/10.1016/S0921-5093(99)00459-1
29. Brossard, S.; Munroe, P.R.; Tran, A.T.T.; Hyland, M.M. Study of the effects of surface chemistry on splat formation for plasma sprayed NiCr onto stainless steel substrates. Surf Coat Technol 2010, 204, 1599–1607, https://doi.org/10.1016/j.surfcoat.2009.10.008
30. Mutter, M.; Mauer, G.; Mücke, R.; Guillon, O.; Vaßen, R. Correlation of splat morphologies with porosity and residual stress in plasma-sprayed YSZ coatings. Surf Coat Technol 2017, 318, 157–169, https://doi.org/10.1016/j.surfcoat.2016.12.061
31. Nouri, A.; Sola, A. Powder morphology in thermal spraying. J Adv Manuf Process 2019, 1, e10020, https://doi.org/10.1002/amp2.10020
32. Shinde, S. V.; Sampath, S. Interplay between cracking and delamination in incrementally deposited plasma sprayed coatings. Acta Mater 2021, 215, 117074, https://doi.org/10.1016/J.ACTAMAT.2021.117074
33. Latka, L.; Goryachev, S.B.; Kozerski, S.; Pawlowski, L. Sintering of fine particles in suspension plasma sprayed coatings. Materials 2010, 3, 3845–3866, doi:10.3390/ma3073845
34. Sathish, S.; Geetha, M.; Aruna, S.T.; Balaji, N.; Rajam, K.S.; Asokamani, R. Studies on plasma sprayed bi-layered ceramic coating on bio-medical Ti–13Nb–13Zr alloy. Ceram Int 2011, 37, 1333–1339, https://doi.org/10.1016/j.ceramint.2010.12.012
35. Pawlowski, L. Suspension and solution thermal spray coatings. Surf Coat Technol 2009, 203, 2807–2829, https://doi.org/10.1016/j.surfcoat.2009.03.005